Paper Number: **1838**

Title: **Nonlinear Analysis and Preliminary Testing Results of a Hybrid Wing Body Center Section Test Article**

Authors: Adam Przekop
Dawn C. Jegley
Marshall Rouse
Andrew E. Lovejoy
Hsi-Yung T. Wu

(FIRST PAGE OF ARTICLE – *align this to the top of page – leave space blank above ABSTRACT*)

ABSTRACT

A large test article was recently designed, analyzed, fabricated, and successfully tested up to the representative design ultimate loads to demonstrate that stiffened composite panels with through-the-thickness reinforcement are a viable option for the next generation large transport category aircraft, including non-conventional configurations such as the hybrid wing body. This paper focuses on finite element analysis and test data correlation of the hybrid wing body center section test article under mechanical, pressure and combined load conditions. Good agreement between predictive nonlinear finite element analysis and test data is found. Results indicate that a geometrically nonlinear analysis is needed to accurately capture the behavior of the non-circular pressurized and highly-stressed structure when the design approach permits local buckling.

INTRODUCTION

The primary structural concept being pursued as an important component of next generation airframe technology under the NASA Environmentally Responsible Aviation (ERA) Project is the Pultruded Rod Stitched Efficient Unitized Structure (PRSEUS) [1-17], illustrated in Figure 1. This concept is being developed in a partnership between NASA and The Boeing Company (Boeing) for application to future transport aircraft with the goal of developing lighter structure so that the aircraft will require less fuel and produce fewer pollutants. The PRSEUS structure is highly integrated, structurally efficient, and has damage-arresting capabilities. In this concept, a stitched carbon-epoxy material system is used. By stitching through the thickness of a dry material system, the labor associated with panel fabrication and assembly can be significantly reduced. When stitching through the thickness of pre-stacked skin, stringers, and frames, the need for mechanical fasteners is almost

Adam Przekop, NASA Langley Research Center, Hampton, Virginia 23681-2199, U.S.A.
Dawn C. Jegley, NASA Langley Research Center, Hampton, Virginia 23681-2199, U.S.A.
Marshall Rouse, NASA Langley Research Center, Hampton, Virginia 23681-2199, U.S.A.
Andrew E. Lovejoy, NASA Langley Research Center, Hampton, Virginia 23681-2199, U.S.A.
Hsi-Yung T. Wu, Boeing Research and Technology, Huntington Beach, California 92647-2048, U.S.A.

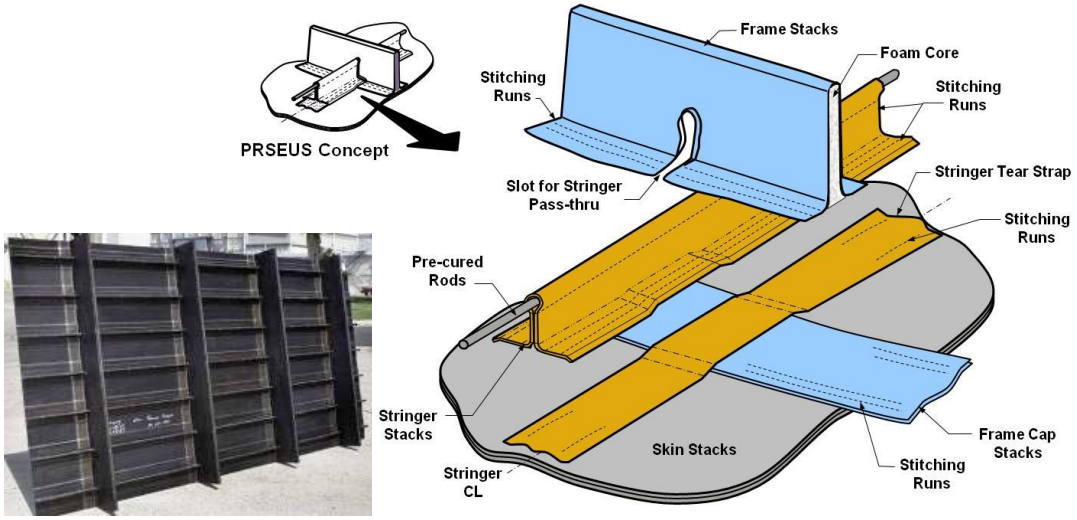

Figure 1. PRSEUS: (a) sample flat panel and (b) general assembly concept.

eliminated. In addition, stitching reduces delamination and improves damage tolerance, allowing for a lighter structure with more gradual failures than traditional layered composites which do not have through-the-thickness reinforcement.

The PRSEUS concept consists of carbon-epoxy panels fabricated from dry components stitched together, after which the resin is infused in an oven while the panel is subjected to vacuum pressure. Skins, flanges, and webs are composed of layers of carbon material that are knitted into multi-ply stacks. A single stack has the thickness of 0.052 in. and comprises seven plies with stacking sequence [+45, -45, 0, 90, 0, -45, +45] and percentage of the 0, 45 and 90-degree fibers equal to 44.9, 42.9, and 12.2, respectively. Several knitted stacks are used to build up the desired thickness and configuration. Stiffener flanges are stitched to the skin using Vectran thread and no mechanical fasteners are used for joining. To maintain the panel geometry during fabrication, first stiffeners and then the skin are placed in a tool for stitching prior to moving the assembly to a curing tool for consolidation in the oven. The stiffeners running in the axial direction (stringers) consist of webs with unidirectional carbon fiber rods at the top of the web. The stack material forming the stiffener web overwraps the rod to form the stiffener cap. The stiffeners in the lateral direction (frames) are foam-filled sandwich structures. The manufacturing process is described in detail in ref. [6].

Numerous articles utilizing the PRSEUS concept have been built and tested. However, typically only individual load conditions such as tension [9,13], compression [7,9,12] or pressure [8,9,11] were applied as a conventional building-block approach was followed. Testing under the combined load environment inherent to the center section of a hybrid wing body (HWB) has not been conducted prior to the tests described in this paper. As illustrated in Figure 2, the top center section of a HWB fuselage is required to sustain loads in each of the three primary directions [15,16], namely stream-wise (Nx), span-wise (Ny), and normal (Nz). Given the specific PRSEUS panel orientation shown in Figure 2, the wing bending loads are carried primarily by the frame members while the fuselage bending loads are carried primarily by the stringers.

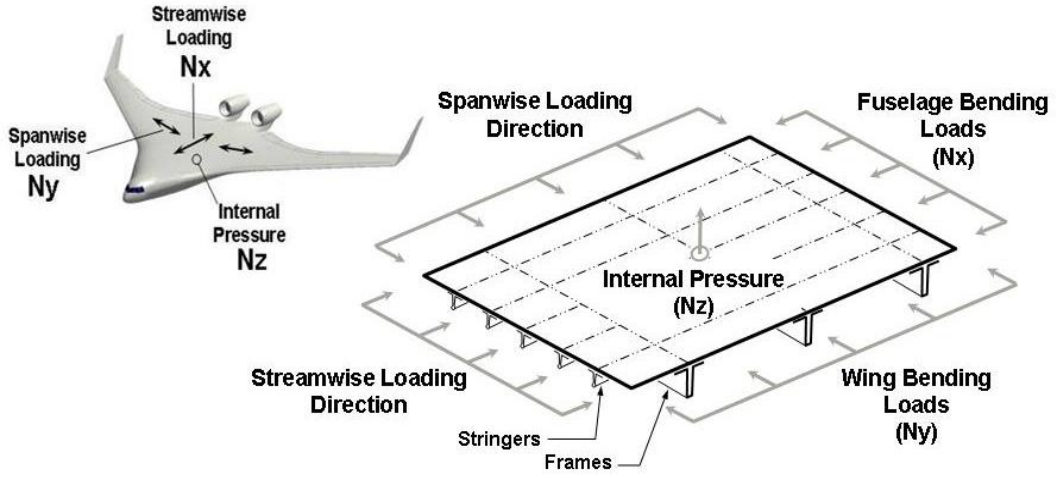

Figure 2. HWB pressure cabin crown panel loading.

As stated before, the overall goal of the development effort was to demonstrate that the PRSEUS concept can meet the demanding requirements of the next generation airframe technology. An important component of this effort was the development and validation of a reliable analysis approach applicable to a HWB configuration built using the PRSEUS concept. A key element of this component was the afore-mentioned testing performed at the Combined Loads Test System (COLTS) Facility [18] located at the NASA Langley Research Center (LaRC). Thus, the objective of the testing was not only the demonstration that the test article could withstand the required loads, but also, the acquisition of test data for validation of analysis methodology.

To achieve the program objectives, the design of a large test article was undertaken by the ERA Project [10,14,17]. The test article, shown in Figure 3, is representative of an 80%-scale center fuselage section of a HWB aircraft and, therefore, is suitable for structural performance evaluation under a combined loading environment where the multi-axial in-plane loads (Nx and Ny) are combined with internal pressure loading (Nz). The test article is approximately 30-feet long, 14-feet tall, and 7-feet wide. The exterior shell and floor comprise 11 PRSEUS panels, and the interior ribs comprise four composite sandwich panels. As shown in Figure 3, the 11 PRSEUS panels are: one crown, one floor, one center keel, two side keels (left and right), two upper bulkheads (forward and aft), two lower bulkheads (forward and aft), and two outer ribs (left and right). The four sandwich panels are two upper inner ribs (left and right) and two lower inner ribs (left and right). All of the composite panels are mechanically joined at their edges by metallic fittings and fasteners.

Initially, a linear finite element analysis (FEA) was used to support the HWB test article design effort [19]. A subsequently performed nonlinear analysis demonstrated that geometrically nonlinear analysis was warranted for this unconventional configuration [20]. For sufficiently high internal pressure and/or mechanical loads, energy related to the in-plane strain may become significant compared to the bending strain energy, particularly in thin sections of the structure, such as the minimum gauge skin. To account for this effect, a geometrically nonlinear strain-displacement

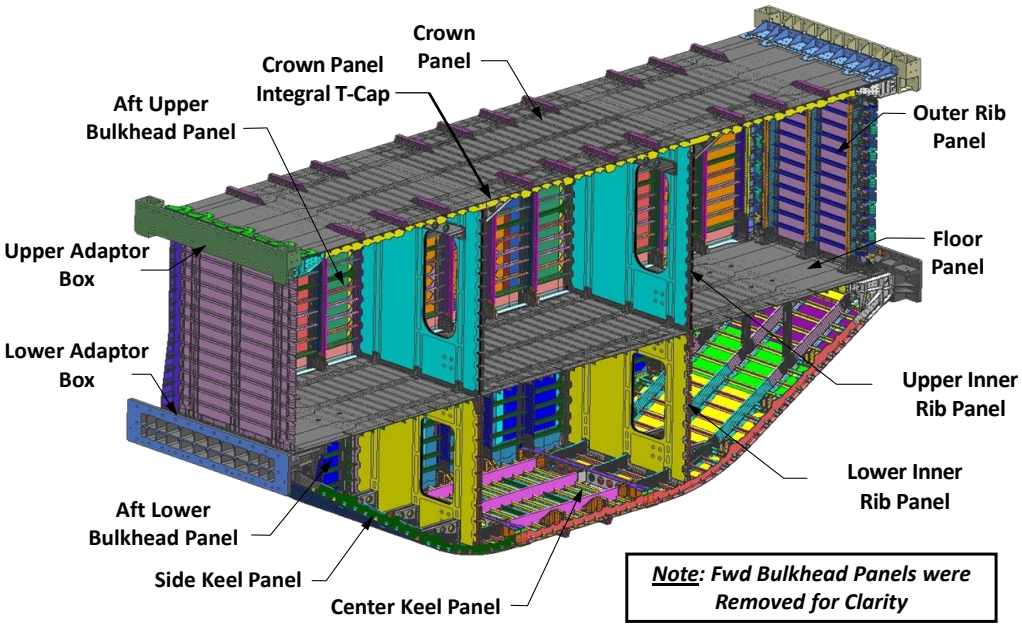

Figure 3. Hybrid wing body center section test article.

relationship that couples out-of-plane and in-plane deformations is required. For the HWB test article this nonlinear coupling specifically has a potential to demonstrate itself in two distinct scenarios. First, local skin buckling is permitted in sections of the structure undergoing compression. Nonlinear analysis is, therefore, needed to accurately capture buckling onset and large post-buckling deformations. Second, under significant pressure load, or pressure load combined with mechanical loads resulting in tension, a significant in-plane tensioning can occur and act as a factor suppressing the out-of-plane deformations. Both behaviors are highlighted in the results section.

FINITE ELEMENT ANALYSIS

A finite element model (FEM) of the composite panels, metallic fittings, mechanical fasteners, and the COLTS test fixture was developed to support the design effort. A nonlinear static solver available in the commercial FEA code MSC Nastran (solution 400) [21] was used to obtain the results presented herein. Shell elements were used to represent composite panels and metallic fittings in the HWB center section test article model shown in Figure 4. The top sections of frames and the pultruded rods in panel stringers are represented by beam elements and connector elements are used to represent fasteners. The loading fixtures of the COLTS Facility are modeled using a combination of shell and beam elements and are annotated in Figure 4 to illustrate boundary conditions and test article mechanical load introduction. The FEM contained approximately 4.5 million degrees-of-freedom. Material properties used in the analysis were the same as those presented in ref. [20].

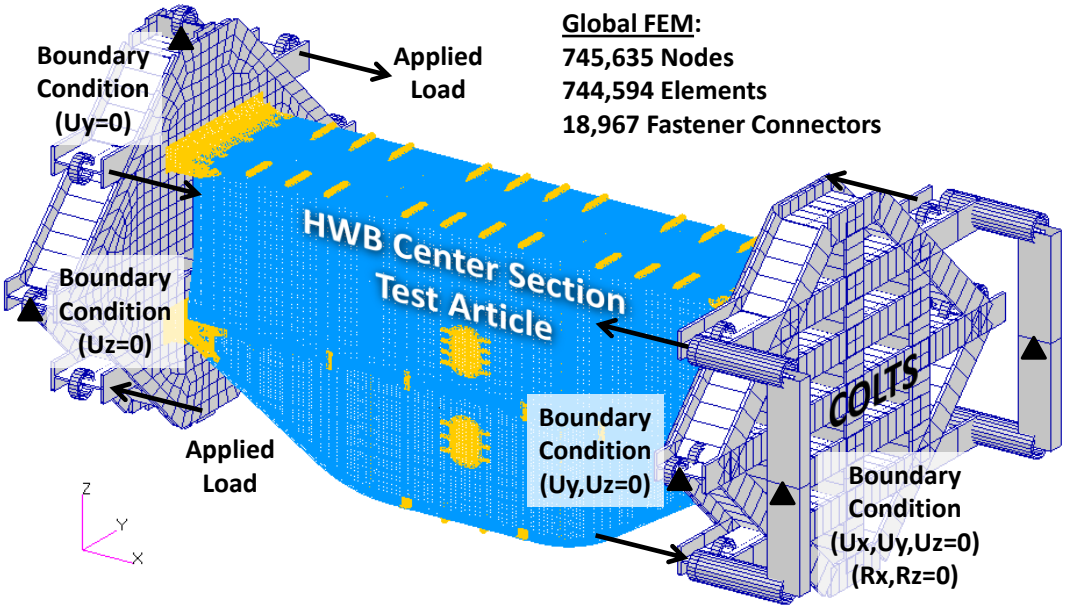

Figure 4. Finite element model of the test article and COLTS test fixture.

Previous vehicle level structural sizing studies [1,4,7] identified several critical loading cases for the center section of the HWB. These are 2.5-g pull up and -1.0-g push over pitch maneuvers, i.e., the maneuvers when the wings bend upward and downward, respectively. Additional load cases include the above maneuver loads combined with the cabin pressurization load, i.e., 2.5-g + 1P and -1.0-g + 1P, respectively. Pressure P is determined based on the intended cruise altitude and in the HWB structural studies is assumed to be 9.2 psi. The four cases and the overpressure condition of 1.33P, equal to 12.2 psi, are design limit loads (DLL). When multiplied by a factor of safety of 1.5 [22], a set of five corresponding design ultimate load (DUL) cases is obtained, where the overpressure condition of 2P is equal to 18.4 psi. Therefore, overall ten load cases, five DLL and five DUL, were of interest in the analysis and testing. Margins of safety (MS), calculated in Equation (1) as

$$MS = (Design\ Value\ /\ Analysis\ or\ Test\ Value) - 1 \quad (1)$$

were obtained for all load cases. The lowest MS were obtained for the 2.5-g + 1P, 2.5-g, and 2P DUL cases [20], so those three load conditions are the focus of the subsequent section.

TEST RESULTS AND COMPARISON WITH PREDICTIONS

Several measurement techniques were used during testing, including: (1) video image correlation in three-dimensions (VIC-3D) [23], (2) strain gage measurements (both unidirectional and rosette), (3) fiber-optic strain measurements, and (4) acoustic emissions measurements. Still photography, video recordings inside and outside of the test article, and audio recordings were also acquired. Due to space limitation, only VIC-3D and strain gage measurements are discussed herein. While VIC-3D

measurements were limited to the crown, bulkhead and keel outer moldline (OML), strain gage data was acquired from both OML and inner moldline (IML) sides of the structure.

In the remainder of this section, the out-of-plane displacement predictions at DUL are introduced first and compared with available full-field measurements obtained using the VIC-3D system. Next, discrete strain FEA results are compared with strain gage measurements at selected characteristic locations on the test article. Displacement plots introduced before are used to define general locations where the strain gage data are compared with FEA predictions, and strain plots include insets showing details of strain gage placement. Strain gage measurements, strains based on linear analysis, and strains based on nonlinear analysis are presented as a function of the load up to DUL. Such plots help to identify sections of the test article, which responded in a nonlinear fashion and at what load level the nonlinear effects became apparent and significant. Results for the 2P load case are shown as a function of the pressure load, and plots for the 2.5-g and the 2.5-g + 1P load cases are shown as a function of the actuator load. In the 2.5-g + 1P load case, pressure was applied proportionally to the actuator load. Minor departures from this nominal relationship in the test are discussed later in this section. The 2.5-g DLL and DUL levels correspond to actuator loads of 159 kips and 238.5 kips, respectively.

The analyses presented in references [19] and [20] were based on a perfect test article while minor manufacturing imperfections of the crown panel OML were included in the analysis described herein. Namely, OML surface repair patches were co-bonded to the crown panel skin as shown in Figure 5 with blue areas. The light blue sections correspond to a single-stack patch thickness and the dark blue sections correspond to a two-stack thickness. Local departures from symmetry in the measured and predicted displacement fields result, at least partially, from these patches. The pink features shown in Figure 5 are external metallic fittings that will be discussed when introducing VIC-3D images.

2.5-g + 1P Design Ultimate Load

DISPLACEMENTS

Under the 2.5-g + 1P DUL case, the top of the test article is compressed by the mechanical loading while the bottom section is tensioned, as illustrated in Figure 4. Additionally, the pressure load bows out the external panels. Crown, upper bulkhead, and center keel out-of-plane deformations at DUL are presented in Figures 6 through 8, respectively. In each figure, the larger plot shows the nonlinear FEA prediction of the entire panel and the smaller plot shows the corresponding VIC-3D measurement. The VIC-3D cameras did not have a clear view of any entire panel, so only a portion is shown. Furthermore, due to inherent limitations of the VIC-3D technique, additional areas within the overall acquisition field are blanked out. Most of the measurement gaps along perimeters of the measured displacement field are due to surface discontinuities often caused by non-flush external metallic fittings or the presence of acoustic emission sensors. Gaps away from the perimeter of the measurement are primarily due to strain gages and bolted joints (e.g., in the case of the bulkhead panel attachment to the internal rib). Axes of symmetry and other characteristic features of the panels are drawn in each image to provide points of reference.

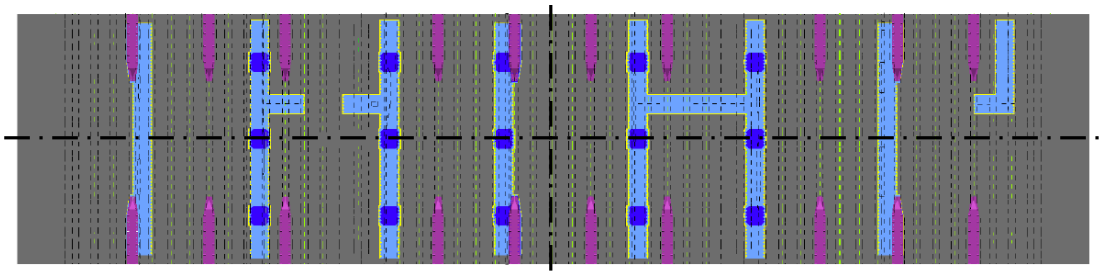

Figure 5. Co-bonded repair patches (blue) and external metallic fittings (pink) of the crown panel.

The crown panel out-of-plane deformation in Figure 6 shows the pillowing of the thin skin sections between stringer and frame flanges in the center section of the panel due to internal pressure. However, in the side sections of the panel some of the skin bays are deformed inwards and some are deformed outwards indicating that the pressure load was not overcoming the alternating skin bay buckling pattern caused by in-plane compression loads. For a periodic structure undergoing local buckling, such as the crown panel, multiple stable post-buckled equilibrium states frequently exist. In the analysis, the specific equilibrium state achieved is typically triggered by numerical perturbations while equilibrium state in a test article is often determined by small geometric and other manufacturing imperfections. Therefore, the local buckling pattern mismatch between analysis and test results seen in the right-hand-side section of the crown panel below the axis of symmetry is not surprising.

The upper bulkhead panel, shown in Figure 7, bows outwards due to the combination of internal pressure loading and, to a lesser extent, the contribution of mechanical compression. Since the unsupported sections of the bulkhead panel are larger than those of the crown panel, two scales of this phenomenon can be observed. Namely, the global deformation of the panel (i.e., between the supporting outer and inner ribs and the crown and floor panels) is accompanied by local deformations at the individual skin bay level. The latter deformations demonstrate themselves as out-of-plane scallops in the deformation contours coinciding with the stringer and frame grid spacing. The global-local effect is the most prominent in the bulkhead panel, but is also observed in the crown panel as shown in Figure 6 and the center keel panel as shown in Figure 8. Overall, good quantitative and qualitative agreement between test and FEA out-of-plane deformation predictions is found.

STRAINS

Crown panel strains are presented in Figure 9. The mid-span strain in the center frame is shown in Figure 9(a) and the location of strain gage on the surface of the crown panel is marked as point A in Figure 6. The strain behavior at this location is representative of the entire crown substructure behavior and is characterized by only mildly nonlinear response. Specifically, the top center frame shows a slightly softening nonlinear response. The measured strains and strains predicted by nonlinear analysis become more negative than those obtained from the linear analysis as the load level is increased.

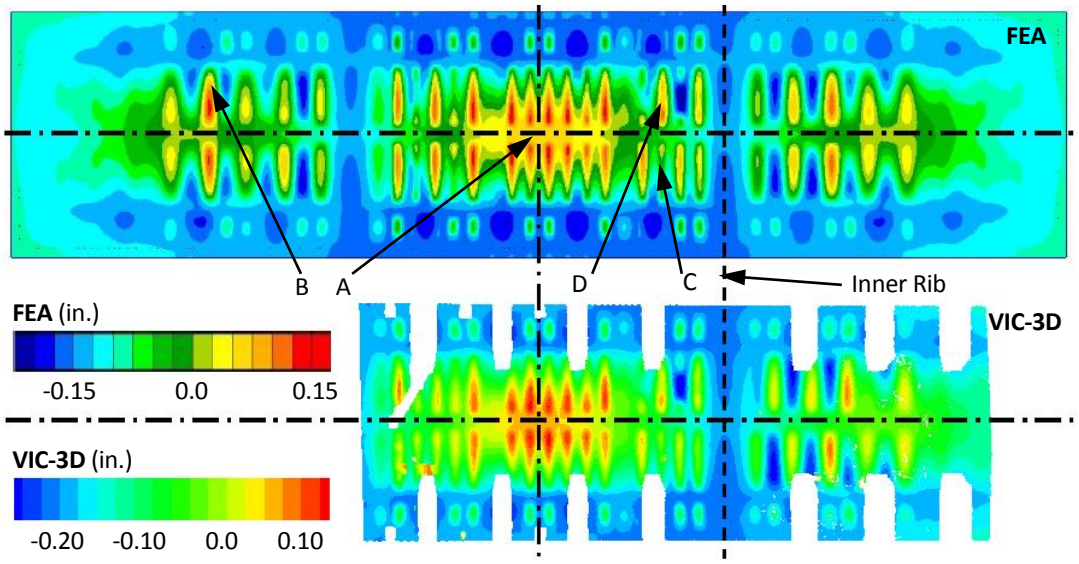

Figure 6. Out-of-plane deformation of the crown panel under 2.5-g + 1P DUL: nonlinear FEA prediction (top) and VIC-3D measurement (bottom).

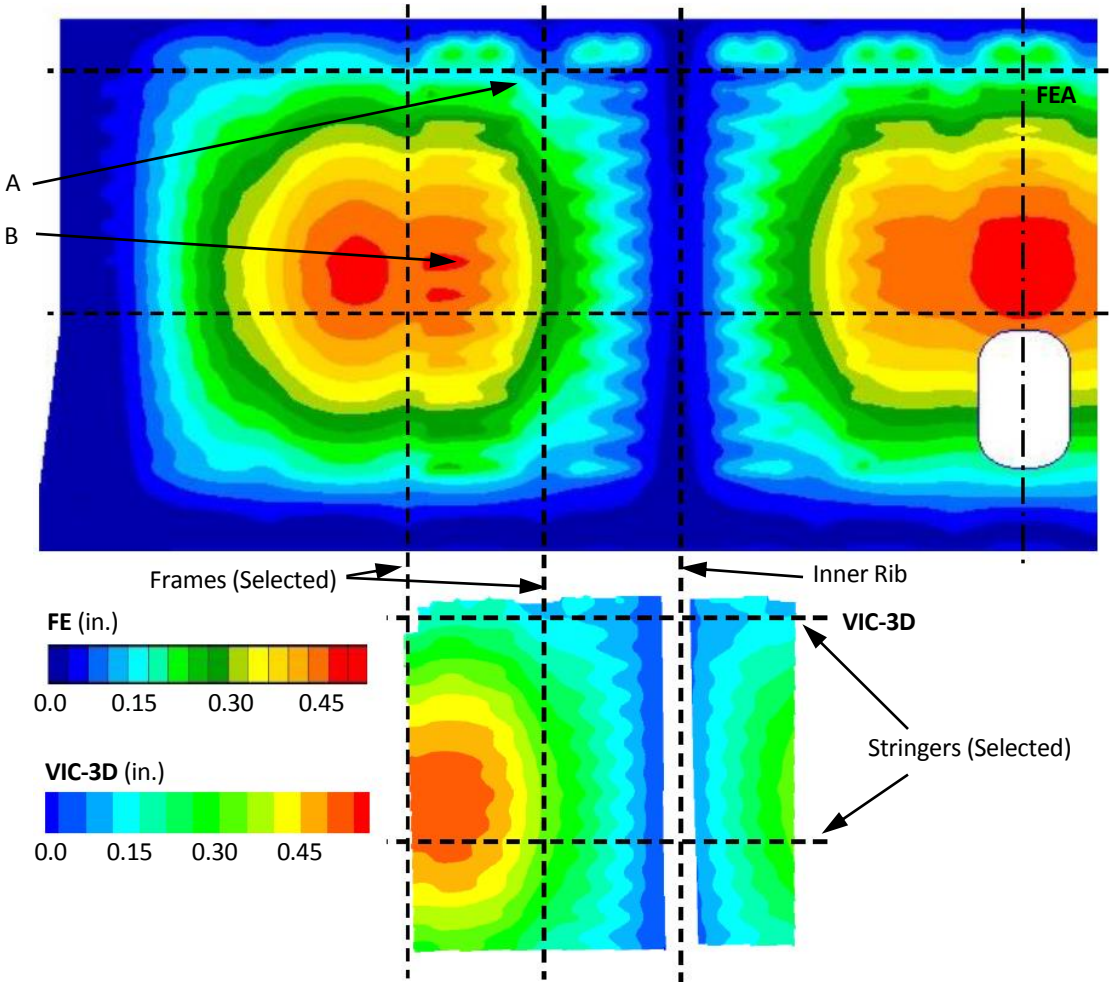

Figure 7. Out-of-plane deformation of the upper bulkhead panel under 2.5-g + 1P DUL: nonlinear FEA prediction (top) and VIC-3D measurement (bottom).

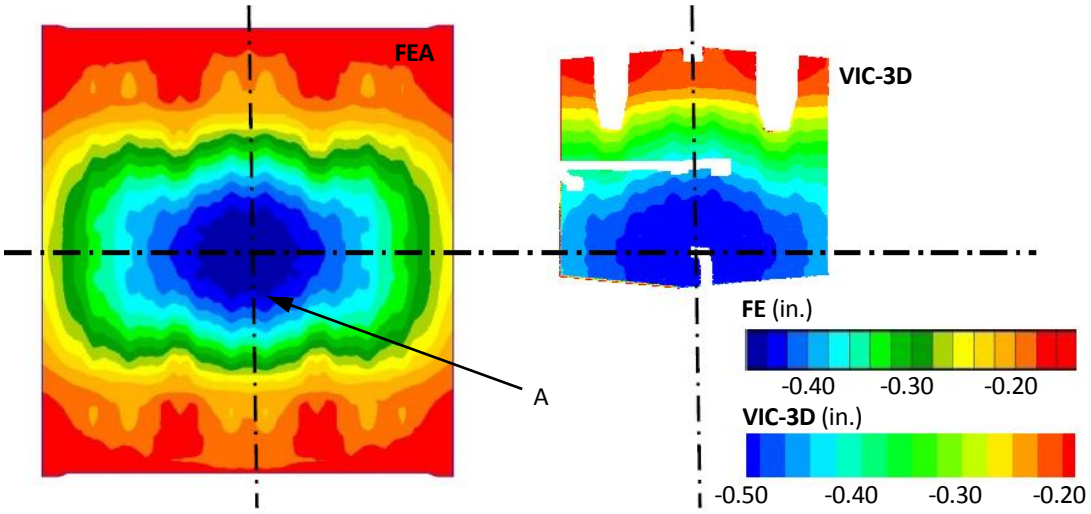

Figure 8. Out-of-plane deformation of the center keel panel under 2.5-g + 1P DUL: nonlinear FEA prediction (left) and VIC-3D measurement (right).

Strains in skin sections of the crown panel show strongly nonlinear behavior. Strains at locations B, C, and D in Figure 6 are shown in Figures 9(b) through 9(d), respectively.

The minimum principal strains at point B are presented in Figure 9(b), where the lowest MS was measured and predicted for the entire structure under 2.5-g + 1P DUL load. This location emphasizes the importance of nonlinear effects in HWB structure as the minimum principal strain begins to grow nonlinearly above approximately 80 kip actuator load (or 1.25-g). At higher loads, the skin bay undergoes large out-of-plane deformation due to the effect of combining strong mechanical compression and normal pressure load. The linear analysis at the DUL under-predicts the strain response at this critical location by a factor of approximately two.

Results from two pairs of back-to-back span-wise crown panel skin gages are presented in Figures 9(c) and 9(d). These locations are characterized by strongly nonlinear response. At the DUL, absolute values of measured strains on both sides of the skin are very similar which indicates that almost the entire strain is due to the bending response component and very little is due to the in-plane component. This result is not surprising as strong mechanical compression coupled with normal pressure loads promotes large out-of-plane deformations resulting in significant bending strains. Linear analysis is unable to correctly predict this response. In both Figure 9(c) and 9(d), the strain gage predictions are negative on both skin sides (one strain is significantly negative, the other one is much smaller) which effectively means that the linear analysis produces comparable bending and in-plane strain contributions. Therefore, the linear results are quantitatively inaccurate and the response mechanism is not properly captured in a qualitative manner.

Better relative comparison of nonlinear FEA results with test data is typically achieved at higher load levels and is shown in Figures 9(c) and 9(d). At least two factors can be relevant to this observation. First, the FEM is based on flat panels with perfectly uniform thickness. The VIC-3D system indicated that the manufacturing imperfections in skin sections can be on the order of the single-stack laminate thickness. Linear

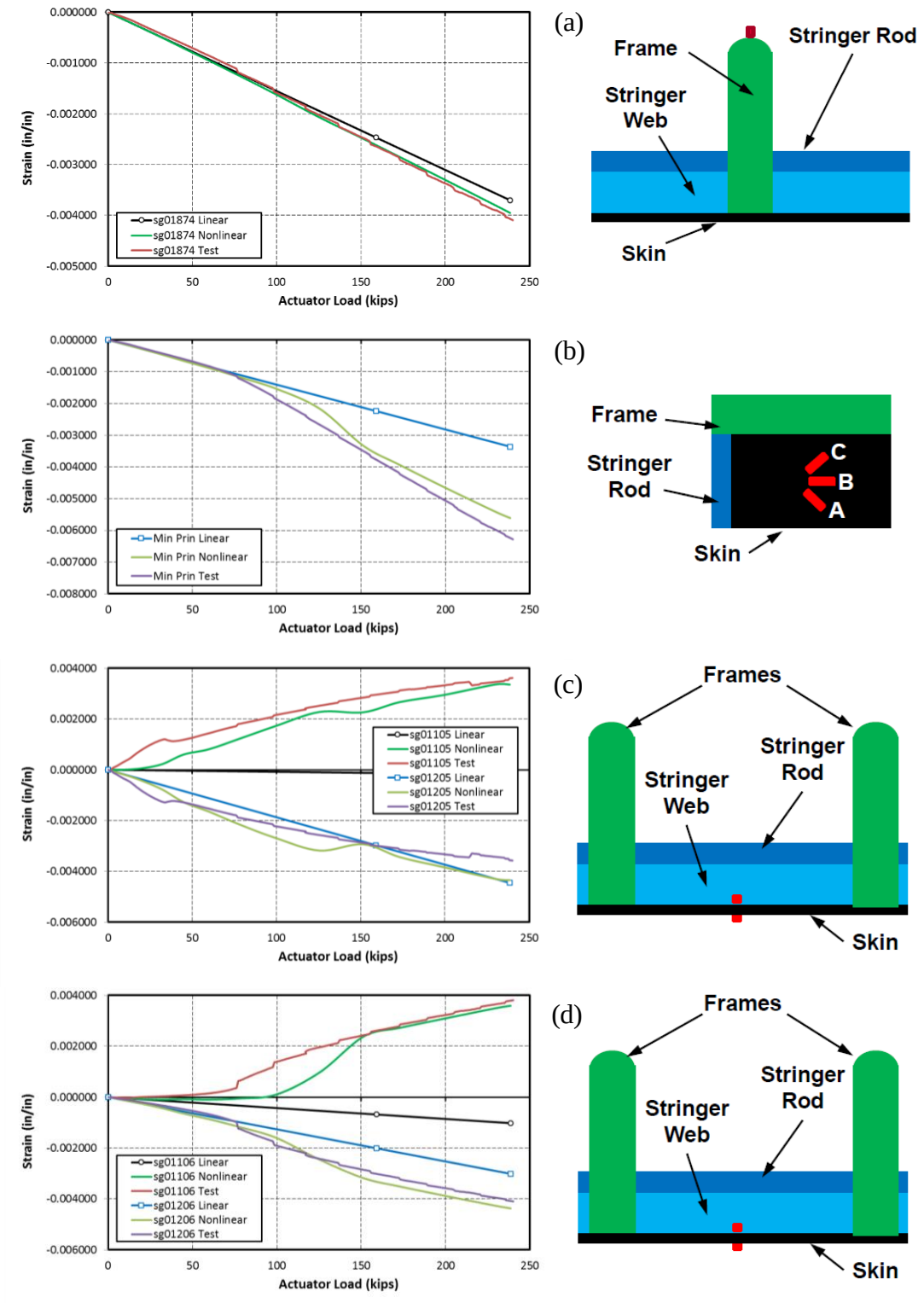

Figure 9. Crown panel strains in selected locations under 2.5-g +1P DUL.

stiffness of perfectly flat and slightly curved skin section is different, and until nonlinear stiffness effects dominate the response at higher load levels, the differences due to this factor can be significant and dominant. Second, in the FEA, mechanical and pressure loads were ramped up proportionally throughout the entire analysis load range. During

the test, however, the pressure loading tracked the applied mechanical load only within certain tolerance. This tolerance, in relative terms, was wider at the lower load levels.

Since the results for bulkhead substructure showed only mildly nonlinear behavior similar to the crown panel frame behavior discussed before, only two bulkhead skin strain results are discussed herein. Skin location A shown in Figure 7 was instrumented with an OML rosette gage, thus minimum and maximum principal strains were calculated and are shown in Figure 10(a). At this location, the minimum principal strain has an absolute value larger than the maximum principal strain and shows slightly softening nonlinear behavior, i.e., measured and nonlinear results are more negative than the linear analysis results. Location B was instrumented with a pair of unidirectional back-to-back gages in the frame direction and these strains are shown in Figure 10(b). Both back-to-back gages show hardening behavior, i.e., measured and nonlinear results are enveloped by linear results that are over-conservative. To investigate why certain sections of the upper bulkhead skin respond in a softening and some in a hardening nonlinear fashion, consider the difference between the locations of points A and B in Figure 7. Location A is close to the crown panel and, therefore, is being compressed with mechanical load similar to the one acting on the crown panel. Since location A is close to the T-cap of the crown panel (the khaki feature seen on the longer edge of the crown panel in Figure 3), the global out-of-plane deformation due to pressure loading is relatively small, and only individual skin bay bowing and, consequently, stretching of the skin influences the response. The two factors partially cancel out, resulting in only mildly nonlinear softening. Location B is approximately half way between the crown and the floor panels, i.e., significantly closer to the neutral bending axis of the test article than location A. Location B, thus, is not subjected to strong mechanical compressive load. At the same time, the out-of-plane deformation is significant at this location because this location is further away from other supports such as crown and floor panels and inner and outer ribs. Consequently, pressure-induced stretching is more significant and results in pronounced hardening nonlinear response. A very similar argument can also be made for the center keel panel skin response shown in Figure 11. Point A in Figure 8 shows the location of two unidirectional back-to-back span-wise gages plotted in Figure 11. The center keel panel is stretched span-wise by the mechanical load and the pressure load only magnifies this tension load. Therefore, the in-plane stretching tends to suppress out-of-plane deformation and, as a result, measured and nonlinear analysis strains are appreciably smaller than those obtained from the linear analysis.

2.5-g Design Ultimate Load

DISPLACEMENTS

Under the 2.5-g DUL, the top of the test article is compressed by the mechanical load, as illustrated in Figure 4. Crown panel and upper bulkhead out-of-plane deformations at DUL are presented in Figures 12 through 13, respectively. The crown panel out-of-plane deformation shows fully developed buckling at most of the individual skin bays throughout the entire span of the panel. Some of the local buckling deformations differ in terms of inward and outward directions between the measurement and the FEA prediction. The explanation of this phenomenon for the 2.5-g + 1P load case is also applicable to the 2.5-g load case.

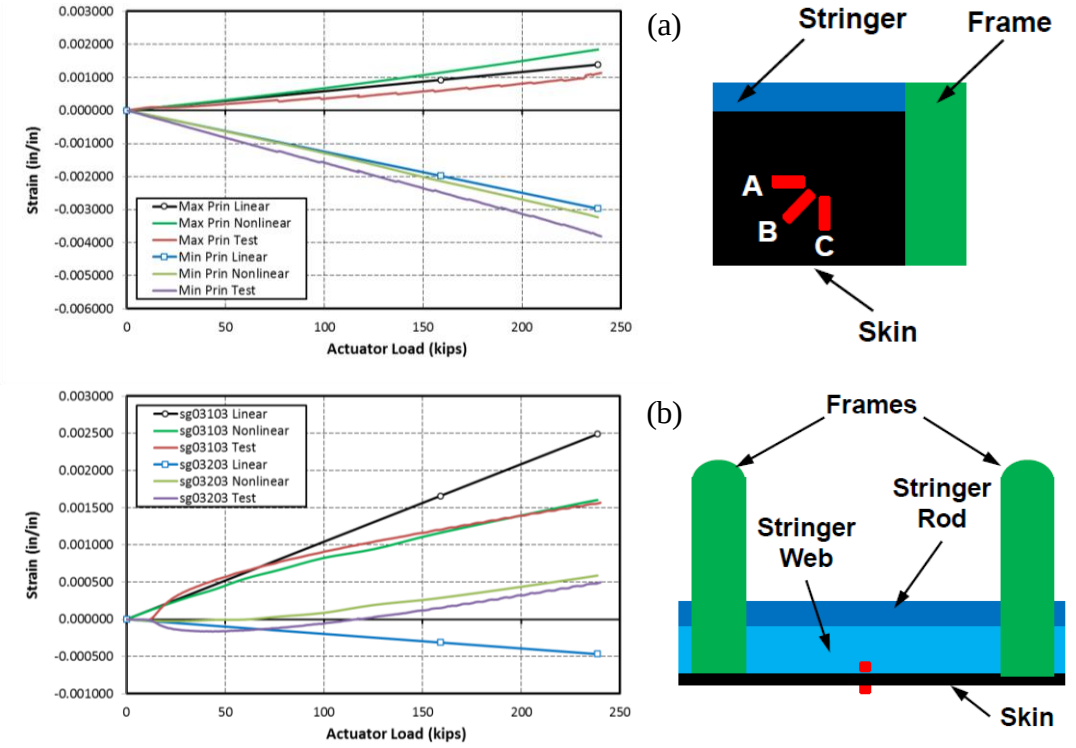

Figure 10. Upper bulkhead skin strains in selected location under 2.5-g +1P DUL.

Some of the skin bays in the upper bulkhead panel also undergo buckling. These regions are primarily skin sections located in the top section of the bulkhead panel close to the attachment of the bulkhead panel to the crown panel, as seen in Figure 13. The scalloping shape of the T-cap, shown in Figure 3, obstructs the view of the topmost skin bays, as apparent in the VIC-3D image, but the full extent of the buckling in these bays can be seen in the FEA results.

The upper bulkhead buckling pattern is different from that of the crown panel. In the crown panel, each skin bay buckling is developed similar to a single semi-sine shape while in the top section of the upper bulkhead, the dominant shapes typically contain three or four semi-sine waves which are additionally skewed. This behavior is the result of the in-plane shear to which the upper bulkhead panel is subjected. Effectively, the top edge of each buckled skin bay in the bulkhead is compressed more than the bottom

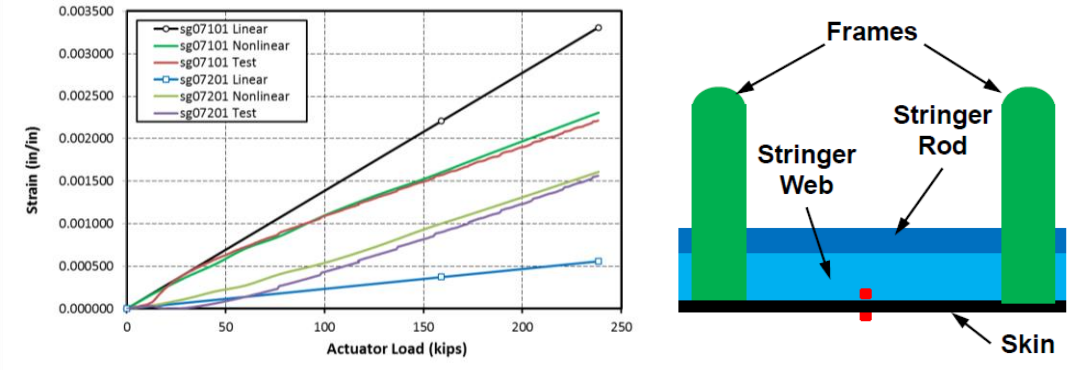

Figure 11. Center keel skin strains at selected location under 2.5-g +1P DUL.

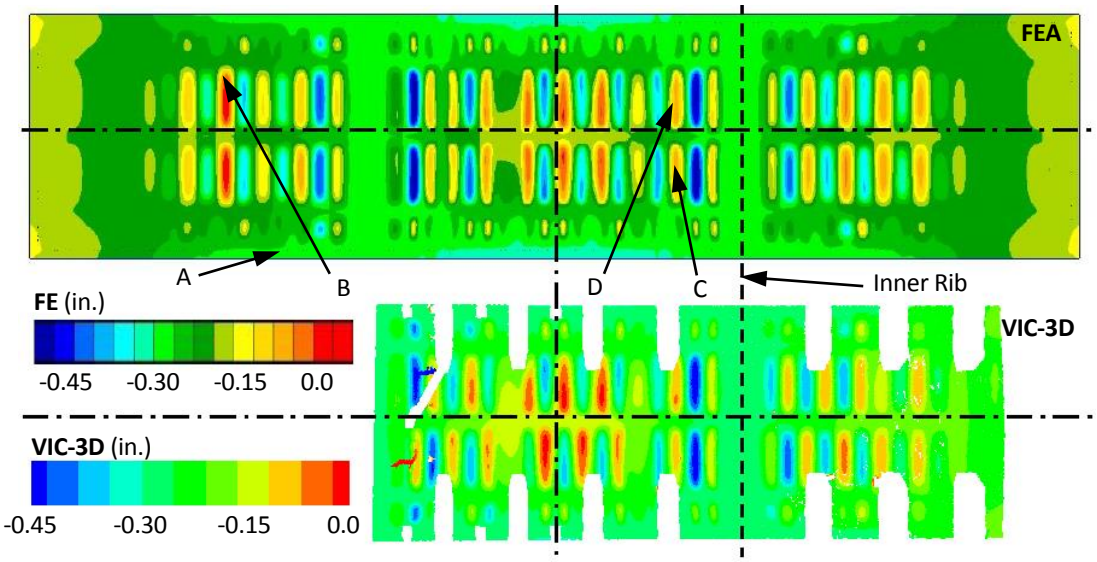

Figure 12. Out-of-plane deformation of the crown panel under 2.5-g DUL: nonlinear FEA prediction (top) and VIC-3D measurement (bottom).

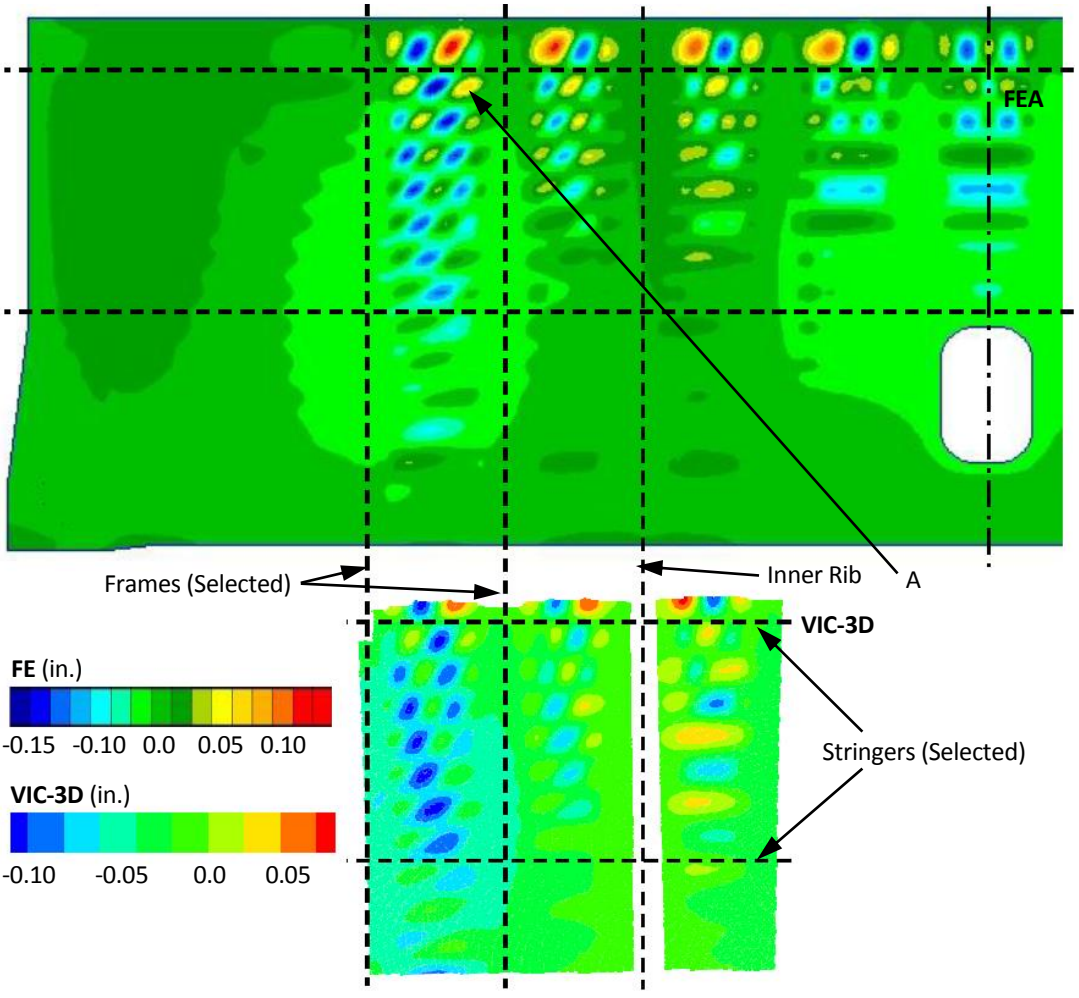

Figure 13. Out-of-plane deformation of the upper bulkhead panel under 2.5-g DUL: nonlinear FEA prediction (top) and VIC-3D measurement (bottom).

edge of the same bay simply by the virtue that the top edge is closer to the crown panel and further away from the neutral bending axis of the entire structure. The skin buckling does not occur in the proximity of the floor panel, i.e., in the direct proximity of the neutral bending axis and in the section of the bulkhead to the left of the most-left dashed line. In this section, the bulkhead panel skin thickness is increased from one to two stacks (i.e., from 0.052 in. to 0.104 in.). Similar to the previous load case, overall good quantitative and qualitative agreement of the out-of-plane deformations is found.

STRAINS

A set of strain results offered for the 2.5-g case is similar to the results introduced before for the 2.5-g + 1P load case. Since the overall response characteristic of the center frame mid-span location is very similar in both 2.5-g and 2.5-g + 1P load cases, an off-center location on the crown panel T-cap is examined instead and is shown in Figure 14(a). The location of the span-wise installed T-cap gage projected on the surface of the crown panel corresponds to point A in Figure 12. Crown panel T-caps are important features of the HWB test article as they not only attach upper bulkheads to the crown panel, but simultaneously carry span-wise loads similar to those transferred by frames. Accurately predicting strains in crown panel T-caps is vital as multiple bolted joints in the T-cap require bypass strain values to be crossed-checked against bearing stresses present in fastener holes as interaction of both influences load carrying capability of the structure. The compressive strains in the T-cap shown in Figure 14(a) are characterized by almost linear dependence relative to the applied load. That relationship is not the case for the three skin locations presented in Figures 14(b) through 14(d) and shown as points B, C and D in Figure 12, respectively.

The minimum principal strain shown in Figure 14(b) displays strongly nonlinear softening response characteristic, qualitatively similar to that presented in Figure 9(b) but with a slightly lower strain level. The more moderate strain level can be attributed to the absence of the pressure loading, even though the response to the mechanical and pressure load components cannot be simply superpositioned in the post-buckled regime. The results for two pairs of skin back-to back span-wise strain gages are presented in Figures 14(c) and 14(d). The test and nonlinear analysis results characteristics are also similar to those shown in Figures 9(c) and 9(d) discussed for the 2.5-g + 1P load case. Note however, that they both differ even further from the linear analysis results. Very small strain differences between the linear strain predictions on both skin sides indicate that the compressive in-plane strain strongly dominates the response and contribution of the bending strain is very small. Both test and nonlinear results, however, point to a different response characteristic. Namely, since the strain gages on both side of the skin have comparable absolute values but opposite signs, in actuality the response is strongly dominated by the bending strain with a very small contribution of the compressive in-plane strain.

The upper bulkhead strains under the 2.5-g load reached the most critical levels in the top sections of the panels affected by skin buckling. Results from two symmetrically placed OML rosettes, one on the aft and one on the forward upper bulkhead panel, are presented in Figures 15(a) and 15(b), respectively, and coincide with location A in Figure 13. Note, that the location A is not at the center of the skin bay but is closer to its corner. The presence of the largest minimum principal strains at this location is

consistent with the out-of-plane deformation field shown in Figure 13, where the individual skin bay buckling shows four semi-sine waves. Strong nonlinear softening of the minimum principal strain response characteristic is clearly identified in both plots.

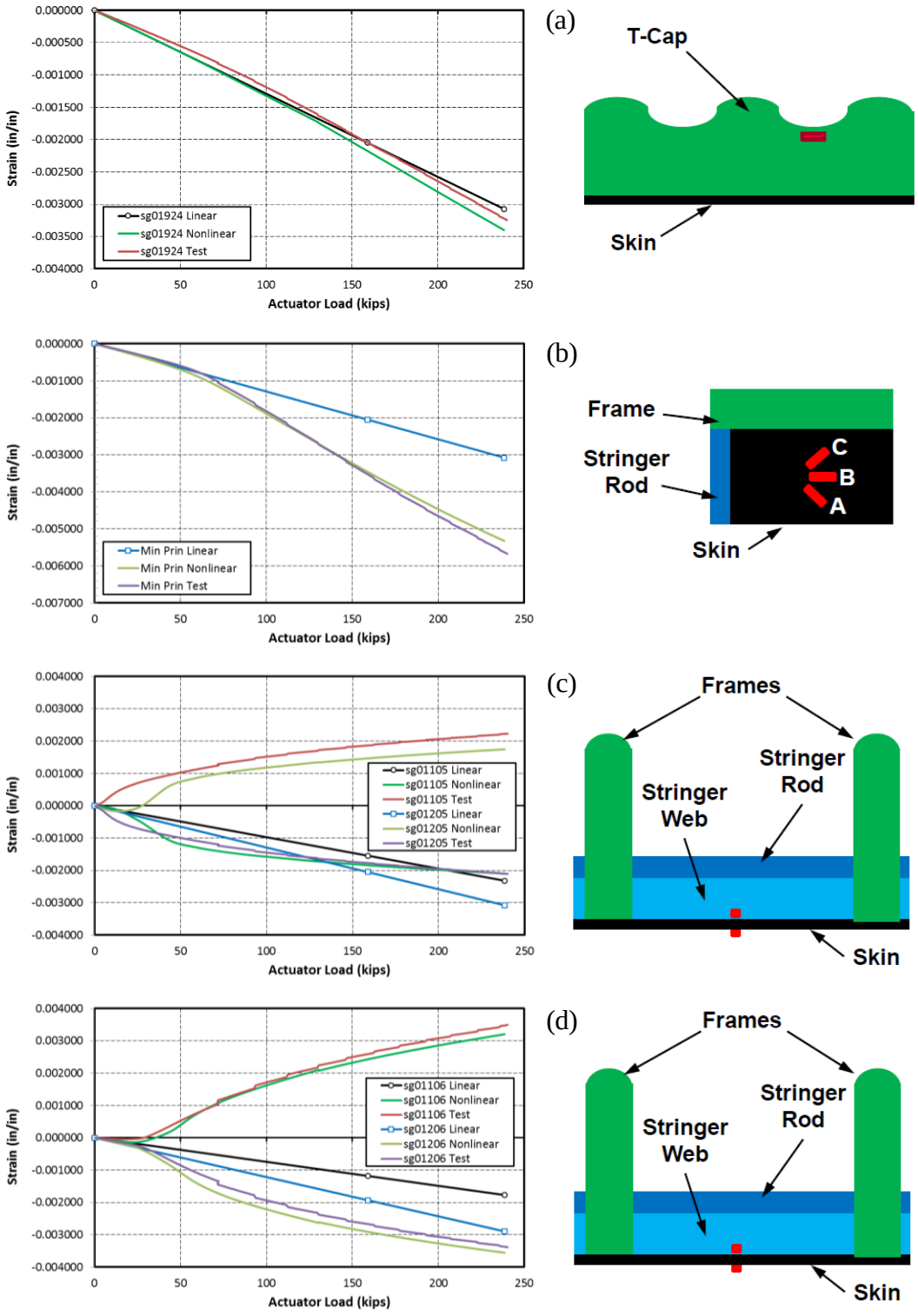

Figure 14. Crown panel strains in selected location under 2.5-g DUL.

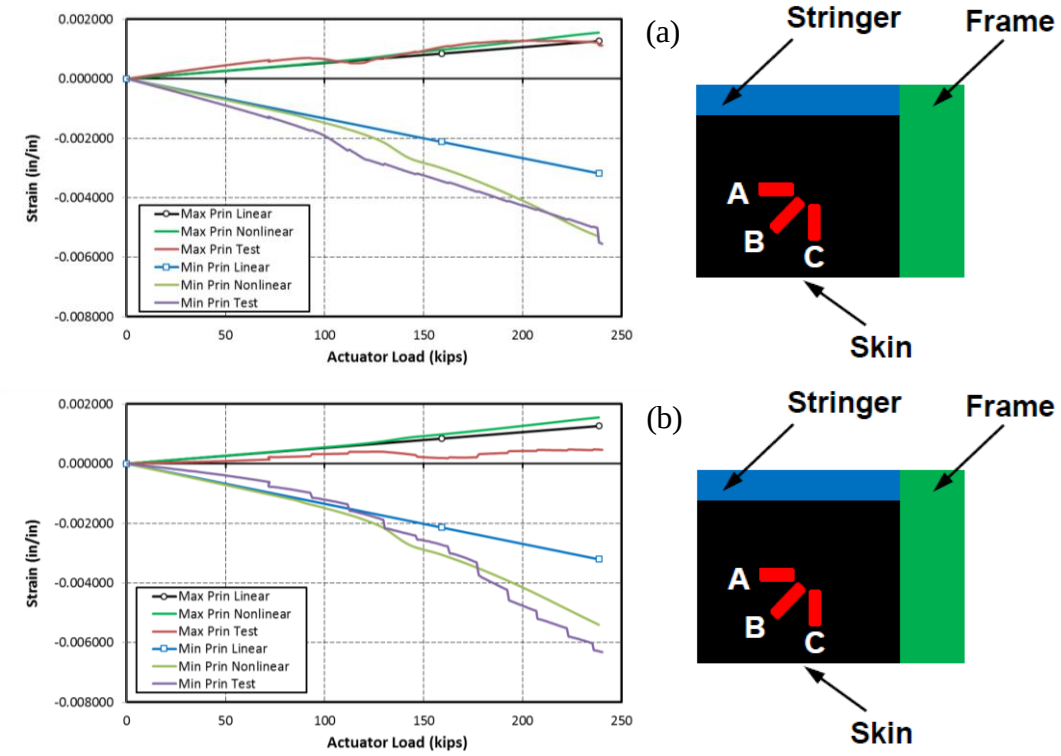

Figure 15. Upper bulkhead strains in selected location under 2.5-g DUL.

2P Design Ultimate Load

DISPLACEMENTS

Under the 2P DUL, all the external panels of the test article bowed out and the largest out-of-plane deformation occurred in the upper bulkhead panels. Crown panel, upper bulkhead and center keel out-of-plane deformations at DUL are presented in Figures 16 through 18, respectively, and show similar patterns. Namely, the displacement is dominated by the global level deformation where attachments to the adjacent panels, both external and internal, act as panel edge restraints. In addition, local deformations associated with individual skin bays are visible as scalloped color contours with spacing coinciding with distances between consecutive frames and stringers. Internal metallic struts (not shown) are also a factor affecting shapes and magnitudes of the displacement fields, but their discussion is omitted here for brevity.

STRAINS

The upper bulkheads are the panels with the largest unsupported sections within the test article, thus are highly strained under the pressure loading. Strain results at the top of the frame and at the minimum gauge skin section are presented in Figures 19(a) and 19(b), respectively, and correspond to locations shown in Figure 17 as points A (projection on the surface of the panel) and B. The top of the frame of the panel that bowls out undergoes compression, as shown in Figure 19(a). Similar to other substructure components, only mildly nonlinear behavior is noted and shows a slight

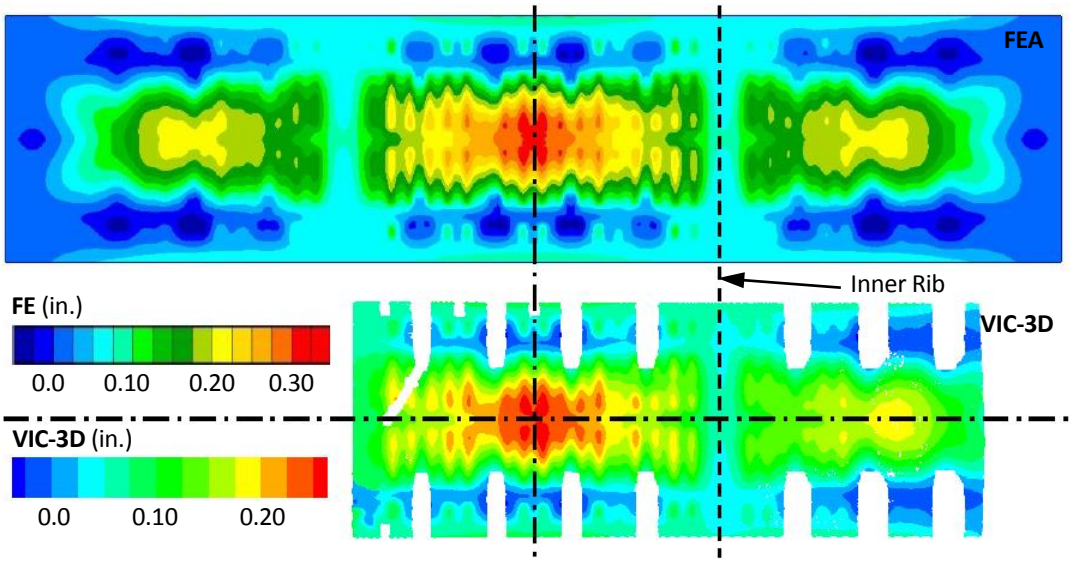

Figure 16. Out-of-plane deformation of the crown panel under 2P DUL: nonlinear FEA prediction (top) and VIC-3D measurement (bottom).

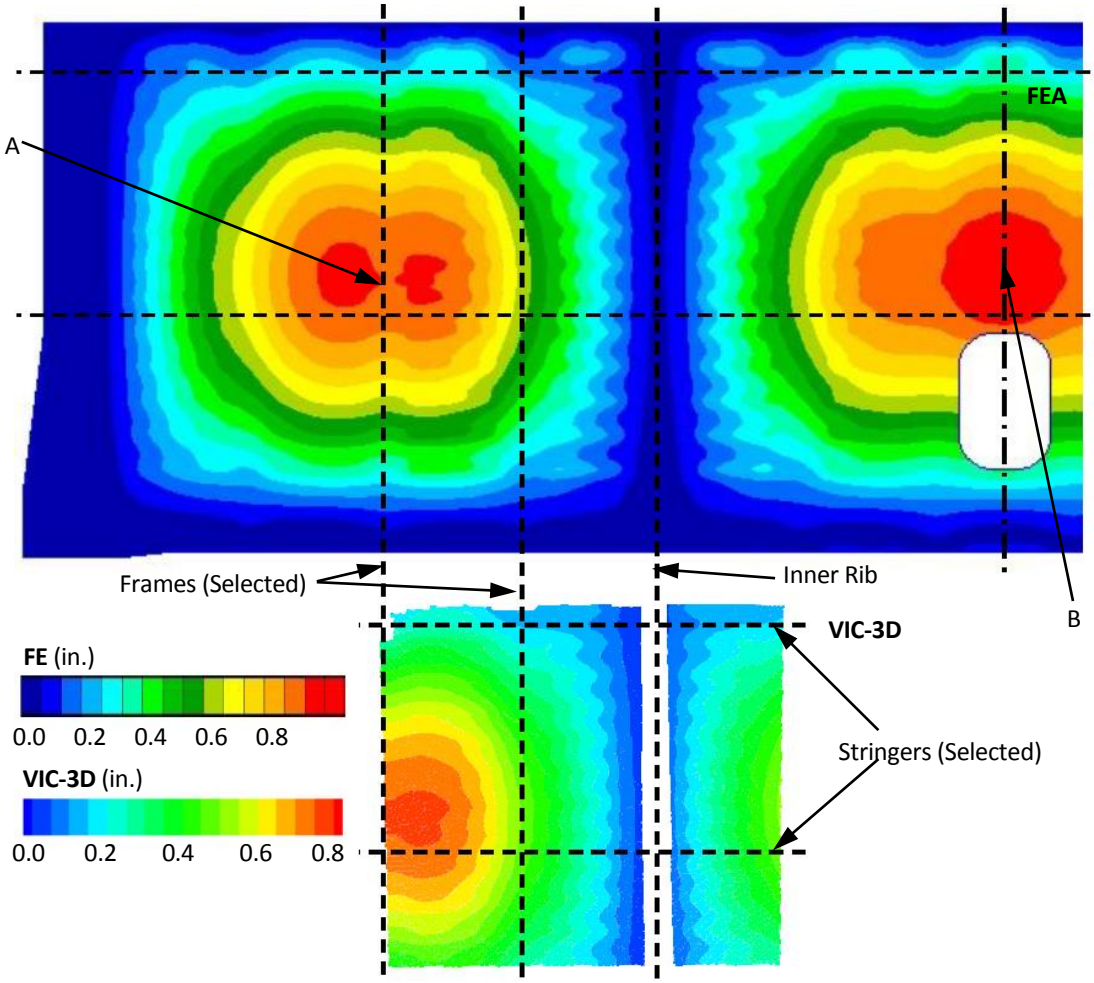

Figure 17. Out-of-plane deformation of the upper bulkhead panel under 2P DUL: nonlinear FEA prediction (top) and VIC-3D measurement (bottom).

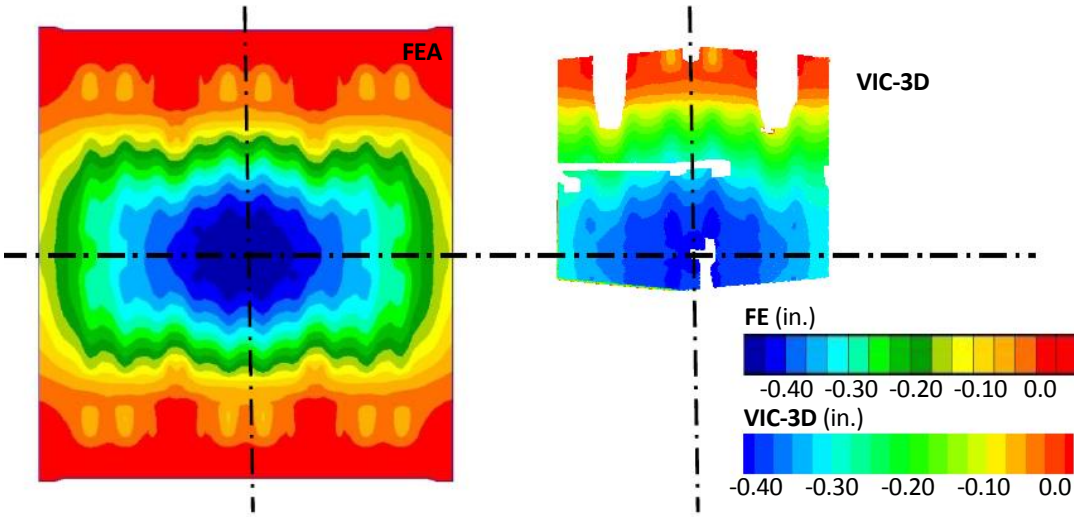

Figure 18. Out-of-plane deformation of the center keel panel under 2P DUL: nonlinear FEA prediction (left) and VIC-3D measurement (right).

hardening characteristic. Skin response, shown in Figure 19(b) for a pair of back-to-back gages in the frame direction, shows appreciably stronger nonlinearity driven, as in the previous such cases, by the low bending stiffness of the minimum gauge skin. This factor promotes early onset of significant in-plane stretching that in turn demonstrates itself in the hardening response, very similar to the response identified for the 2.5-g + 1P DUL case shown in Figure 10(b).

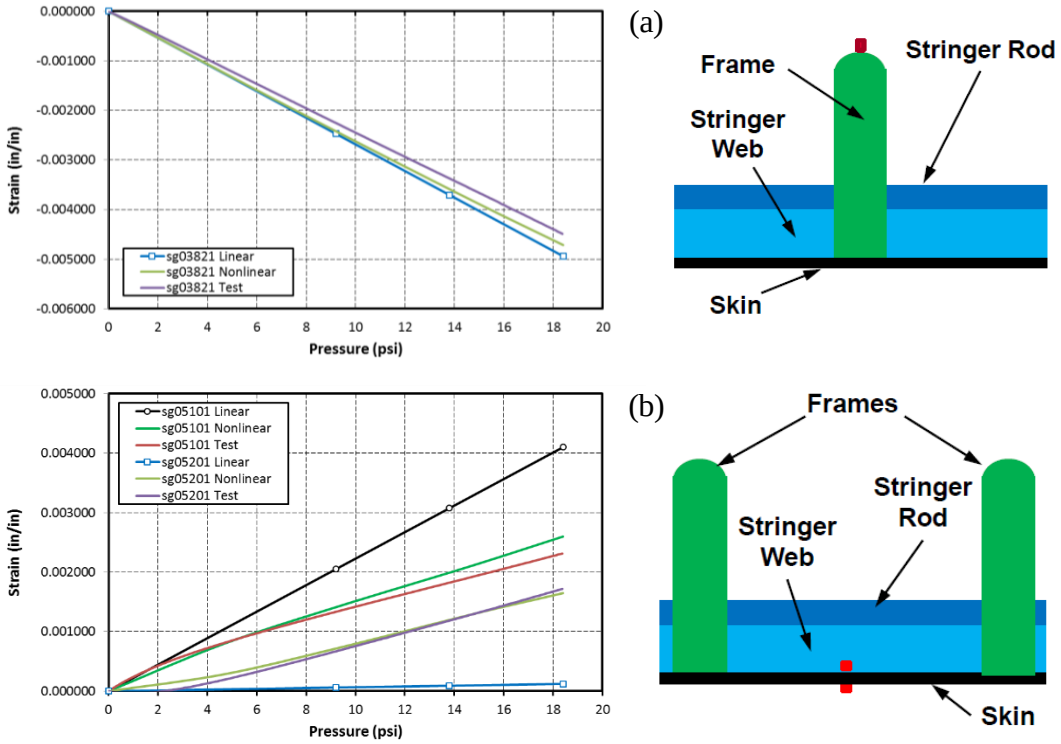

Figure 19. Upper bulkhead strains in selected location under 2P DUL.

CONCLUDING REMARKS

The HWB center section test article was successfully tested under five loading scenarios up to the design ultimate load levels demonstrating the viability of the PRSEUS concept as the next generation airframe technology enabling non-conventional aircraft configurations and/or a weight-efficient approach to design of conventional tube-and-wing airframes. Predictive nonlinear FEA results compared very favorably with the test data and demonstrated that accounting for the geometrically nonlinear effects was required in the analysis. While substructure components responded only in a mildly nonlinear fashion, strong nonlinear behavior was identified in several thin surface skin sections of the test article. Both softening and hardening types of nonlinear response (i.e., larger or smaller relative to the linear analysis, respectively) were identified. The surface skin sections of the structure exhibited sensitivity of the response to initial manufacturing imperfections, especially at the lower load ranges where the nonlinear effects were not prominently developed. These manufacturing imperfections and nonlinear effects were found to be particularly important under compressive loads in sections of the structure susceptible to buckling at low loads.

REFERENCES

1. Li, V. P. and A. Velicki. 2008. "Advanced PRSEUS Structural Concept Design and Optimization," *Proceedings of the 12th AIAA/ISSMO Multidisciplinary Analysis and Optimization Conference*, AIAA-2008-5840, Victoria, BC, Canada, September 10-12, 2008.
2. Jegley, D. C., A. Velicki, and D. A. Hansen. 2008. "Structural Efficiency of Stitched Rod-Stiffened Composite Panels with Stiffener Crippling," *Proceedings of the 49th AIAA/ASME/ASCE/AHS/ASC Structures, Structural Dynamics and Materials Conference*, AIAA-2008-2170, Schaumburg, IL, April 7-10, 2008.
3. Velicki, A., P. J. Thrash, and D. C. Jegley. 2009. "Airframe Development for the Hybrid Wing Body Aircraft," *Proceedings of the 47th AIAA Aerospace Sciences Meeting Including The New Horizons Forum and Aerospace Exposition*, AIAA-2009-932, Orlando, FL, January 5-9, 2009.
4. Yovanof, N. P., A. Velicki, and V. P. Li. 2009. "Advanced Structural Stability Analysis of a Nonlinear BWB-Shaped Vehicle," *Proceedings of the 50th AIAA/ASME/ASCE/AHS/ASC Structures, Structural Dynamics and Materials Conference*, AIAA-2009-2452, Palm Springs, CA, April 4-7, 2009.
5. Velicki, A. and P. J. Thrash. 2008. "Advanced Structural Concept Development Using Stitched Composites," *Proceedings of the 49th AIAA/ASME/ASCE/AHS/ASC Structures, Structural Dynamics and Materials Conference*, AIAA-2008-2329, Schaumburg, IL, April 7-10, 2008.
6. Thrash, P. J. 2014. "Manufacturing of a Stitched Resin Infused Fuselage Test Article," *Proceedings of the Composites and Advanced Materials Expo*, Orlando, FL, October 13-16, 2014.
7. Velicki, A. 2009. "Damage Arresting Composites for Shaped Vehicles, Phase I Final Report," NASA CR-2009-215932, NASA Langley Research Center, Hampton, VA, September 2009.
8. Lovejoy, A. E., M. Rouse, K. A. Linton, and V. P. Li. 2011. "Pressure Testing of a Minimum Gauge PRSEUS Panel," *Proceedings of the 52nd AIAA/ASME/ASCE/AHS/ASC Structures, Structural Dynamics and Materials Conference*, AIAA-2011-1813, Denver, CO, April 4-7, 2011.
9. Velicki, A., N. P. Yovanof, J. Baraja, K. A. Linton, V. P. Li, A. Hawley, P. J. Thrash, S. DeCoux, and R. Pickell. 2011. "Damage Arresting Composites for Shaped Vehicles – Phase II Final Report," NASA CR-2011-216880, NASA Langley Research Center, Hampton, VA, January 2011.
10. Velicki, A. and D. C. Jegley. 2011. "PRSEUS Development for the Hybrid Wing Body Aircraft," *Proceedings of the AIAA Centennial of Naval Aviation Forum "100 Years of Achievement and Progress,"* AIAA-2011-7025, Virginia Beach, VA, September 21-22, 2011.

11. Yovanof, N. P., J. Baraja, A. E. Lovejoy, and K. E. Gould. 2012. "Design, Analysis, and Testing of a PRSEUS Pressure Cube to Investigate Assembly Joints," *Proceedings of the 2012 Aircraft Airworthiness and Sustainment Conference*, TP5431, Baltimore, MD, April 2-5, 2012.
12. Yovanof, N. P. and D. C. Jegley. 2011. "Compressive Behavior of Frame-Stiffened Composite Panels," *52th AIAA Structures, Structural Dynamics and Materials Conference*, AIAA-2011-1913, Denver, CO, April 4-7, 2011.
13. Przekop, A. and D. C. Jegley. 2013. "Testing and Analysis Validation of a Metallic Repair Applied to a PRSEUS Tension Panel," *Proceedings of the 54th AIAA/ASME/ASCE/AHS/ASC Structures, Structural Dynamics and Materials Conference*, AIAA-2013-1735, Boston, MA, April 8-11, 2013.
14. Jegley, D. C. and A. Velicki. 2013. "Status of Advanced Stitched Unitized Composite Aircraft Structure," *Proceedings of the 51st AIAA Aerospace Sciences Meeting*, AIAA 2013-0410, Grapevine, TX, January 7-10, 2013.
15. Velicki, A. and P. J. Thrash. 2011. "Damage Arrest Design Approach Using Stitched Composites", *The Aeronautical Journal*, Vol. 115, No. 1174, pp. 789-795, Royal Aeronautical Society, London, UK, December 2011.
16. Bergen, A., J. Bakuckas, A. E. Lovejoy, D. C. Jegley, K. A. Linton, G. Korkosz, J. Awerbuch, and T. Tan. 2011. "Full-Scale Test and Analysis of a PRSEUS Fuselage Panel to Assess Damage-Containment Features," *Proceedings of the 2011 Aircraft Airworthiness and Sustainment Conference*, TP4558, San Diego, CA, April 18-21, 2011.
17. Velicki, A. and P. J. Thrash. 2008. "Blended Wing Body Structural Concept Development," *Proceedings of Aircraft Structural Design Conference*, Liverpool, UK, October 14-16, 2008.
18. Ambur, D. A., M. Rouse, J. H. Starnes, and M. J. Stuart. 1994. "Facilities for Combined Loads Testing of Aircraft Structures to Satisfy Structural Technology Development Requirements," *Proceedings of the 5th Annual Advanced Composites Technology Conference*, Seattle, WA, August 22-26, 1994.
19. Wu, H. T., P. Shaw, and A. Przekop. 2013. "Analysis of a Hybrid Wing Body Center Section Test Article," *Proceedings of the 54th AIAA/ASME/ASCE/AHS/ASC Structures, Structural Dynamics and Materials Conference*, AIAA-2013-1734, Boston, MA, April 8-11, 2013.
20. Przekop, A., H. T. Wu, and P. Shaw. 2014. "Nonlinear Finite Element Analysis of a Composite Non-Cylindrical Pressurized Aircraft Fuselage Structure," *Proceedings of the 55th AIAA/ASME/ASCE/AHS/ASC Structures, Structural Dynamics and Materials Conference*, AIAA-2014-1064, National Harbor, MD, January 13-17, 2014.
21. MSC Nastran 2012.2 Quick Reference Guide, MSC Software Corporation, Santa Ana, CA, 2012.
22. Title 14 Code of Federal Regulation, Part 25 "Airworthiness Standards: Transport Category Airplanes," Subpart C "Structure," Electronic Code of Federal Regulations, http://www.ecfr.gov/cgi-bin/text-idx?c=ecfr&tpl=/ecfrbrowse/Title14/14cfr25_main_02.tpl
23. McGowan, D. M., D. R. Ambur, and S. R. McNeil. 2003. "Full-field Structural Response of Composite Structures: Analysis and Experiment," *Proceedings of the 44th AIAA/ASME/ASCE/AHS/ASC Structures, Structural Dynamics and Materials Conference*, AIAA 2003-1623, Norfolk, VA, April 7-10, 2003.